

Influence of the electronic core polarization on the electric-field gradients in solids

J. Ehmann and M. Fähnle

Max-Planck-Institut für Metallforschung, Heisenbergstrasse 1, D-70569 Stuttgart, Germany

(Received 21 October 1996)

In conventional band-structure calculations it is normally assumed that closed electronic shells have a spherically symmetric charge density. As a consequence of this approximation, these core states give no contribution to the electric-field gradient (efg) at the nuclear site. In the present paper two equivalent methods for the computation of the actual contribution of closed electron shells to the efg are presented. In the first method the potential of the nuclear quadrupole moment is considered as a perturbation for the core electrons, which causes a polarization of the core states, i.e., a deviation of the core-charge density from spherical symmetry. In this case the core contribution to the efg can be calculated with the help of the Sternheimer function $\chi(r)$. The second method considers the nonspherical parts of the effective crystal potential near the nucleus under consideration as a perturbation for the core electrons. These two methods yield identical results for the interaction energy of the nuclear quadrupole moment with the calculated efg. They are compared with alternative treatments of energetically high-lying core states within the framework of the full-potential linearized-augmented-plane-wave method (semicore calculations and use of local orbitals). As test cases we calculate the efg at the nearest-neighbor sites of a substitutional Ni (Fe) atom in Cu (Al) and the efg at a regular lattice site in hexagonal Mg. Additionally, results for the relaxed atomic positions, the efg, and the asymmetry parameters around a substitutional Pd (V) atom in Cu (Al) are presented. [S0163-1829(97)03612-6]

I. INTRODUCTION

In crystals the electric-field gradients (efg's) do not vanish at nuclear sites with noncubic point symmetry. The interaction of the efg with the electric-quadrupole moment of the nuclei leads to quadrupolar splittings of the nuclear energy levels, which can be measured by different techniques [e.g., nuclear magnetic resonance (NMR), nuclear quadrupole resonance, Mössbauer spectroscopy, or perturbed angular correlation; see, for instance, Refs. 1 and 2]. If the nuclear quadrupole moment Q is known, the efg can be deduced from experimentally observed transition frequencies between the nuclear energy levels. The efg is a ground-state property of the system and depends sensitively on the electronic charge distribution in the vicinity of the nucleus under consideration. Therefore, the experimental determination of efg is an important and valuable tool for the investigation of the chemical bonding and electronic structure of solids. Especially important is the investigation of efg's near atomic defects in solids because they serve as "fingerprints" for the identification of the type of defect produced, for instance, by quenching, cold working, or irradiation with fast particles.³

For the case of ionic crystals the calculational method of Sternheimer (for an overview see Ref. 4) is widely accepted. In this method the crystal is conceived as an assembly of point charges surrounding the atom under consideration and the polarization of the core states of this atom by the point charges is accounted for by a Sternheimer factor γ_∞ if the point charges are outside the considered core or by a Sternheimer function $\chi(r)$ otherwise. In metals and semiconductors, however, the actual charge distribution cannot be described by point charges and has to be determined by accurate band-structure calculations within the framework of the density-functional theory of Hohenberg and Kohn⁵ and the local-density approximation.⁶ In most of these calcula-

tions the charge density of the core electrons has been treated for computational reasons as spherically symmetric. As a consequence, there is no core contribution to the efg. Indeed, within the framework of such calculations, accurate or at least fair results for the efg could be obtained, for instance, for hexagonal metals,^{7,8} in dilute copper alloys,⁹ in $\text{YBa}_2\text{Cu}_3\text{O}_x$,¹⁰ and near atomic defects in Al or Cu.^{3,11}

Blaha, Schwarz, and Dederichs⁷ went one step further and tried to describe the polarization of the uppermost atomic core states. They argued that for these states the spatial overlap of the corresponding orbitals at neighboring atoms is very small, but still numerically significant so that they may be described as semicore states within the framework of a full-potential linearized-augmented-plane-wave method (FLAPW). (The polarization of the lower-lying core states was neglected.) They found that the so-obtained core contribution to the efg is negligibly small for most metals. The starting point of our investigations was the suspicion that the basis set used for the FLAPW semicore calculation is probably not flexible enough to describe the polarization of real core states in an appropriate manner and that in reality the core contribution to the efg might be quite substantial, especially close to atomic defects. The alternative methods that we developed are suited to describe the polarization of all real core states, i.e., of all core states that do not contribute to the chemical bonding. In some cases the uppermost core states of the corresponding free atom are spatially extended beyond the Wigner-Seitz sphere in the crystal. To account for the considerable spatial overlap of these orbitals with orbitals from neighboring atoms these extended core states have to be treated as semicore states or valence states in the crystal. Examples are the $3p$ states of Ti,¹² the $4p$ states of Mo,^{13,14} and the $5p$ states of rare-earth atoms.¹⁵⁻¹⁷ For these special cases our calculational methods cannot be applied.

In the following, two methods are developed to describe

the core polarization. In the first method the potential of the nuclear quadrupole moment Q is treated as a perturbation of the spherically symmetric core-charge density. This perturbation induces an additional quadrupole moment in the charge density of the core electrons and it can be demonstrated that the core contribution to the efg can be calculated with the help of the Sternheimer function $\gamma(r)$. In the second method the nonspherical core-charge density is calculated by considering the nonspherical parts of the effective potential in the solid as a perturbation of the core states.

These two methods yield identical results for the interaction energy of the nuclear quadrupole moment with the efg (Sec. II). They clearly demonstrate that, in general, the core contribution to the efg has to be considered in order to obtain a reliable efg.

All calculations in the present paper have been performed with the FLAPW method using the WIEN95 code.¹⁸ Within this code there are two methods to determine the influence of the highest core states (e.g., $3s$ and $3p$ of copper) on the efg (the polarization of lower-lying core states is neglected). These are, on the one hand, semicore calculations¹⁹ (see above) and, on the other hand, the use of local orbitals.^{12,19,20} The reliability and accuracy of these two methods for a description of true core states can be checked by comparison with our calculations and will be discussed thoroughly.

The paper is organized as follows. In Sec. II the general theory involved in the *ab initio* calculation of efg's in solids is outlined. In Sec. III the two methods for the determination of the core contribution to the efg are presented. Section IV A reports the results of calculations of the efg generated by a substitutional nickel (Ni) atom in copper (Cu) with special regard to the influence of the core electrons on the efg. The results for the core contribution to the efg will be compared with the results of FLAPW semicore calculations and calculations using local orbitals. Additionally, we report the results for the relaxed atomic positions and efg's near a substitutional palladium (Pd) atom in Cu. Section IV B deals with the efg near a substitutional iron (Fe) or vanadium (V) atom in aluminum (Al) and Sec. IV C with the efg in hexagonal magnesium (Mg). Section V gives a short discussion and a summary.

II. AB INITIO CALCULATION OF ELECTRIC-FIELD GRADIENTS

The traceless symmetric tensor of the efg at a nucleus in the origin of our coordinate system is defined as

$$V_{ij} = \left. \frac{\partial^2 \Phi}{\partial x_i \partial x_j} \right|_0 - \frac{1}{3} \delta_{ij} \Delta \Phi \Big|_0, \quad (1)$$

where

$$\Phi(\mathbf{r}) = \int \frac{\rho(\mathbf{r}')}{|\mathbf{r} - \mathbf{r}'|} d\mathbf{r}' \quad (2)$$

is the electrostatic potential and $\rho(\mathbf{r})$ the total ground-state charge density of the system. The subscript 0 indicates that all derivatives have to be taken at $\mathbf{r} = \mathbf{0}$. Inserting Eq. (2) into Eq. (1) yields

$$V_{ij} = \int \rho(\mathbf{r}) \left(\frac{3x_i x_j}{r^5} - \frac{\delta_{ij}}{r^3} \right) d\mathbf{r}. \quad (3)$$

Since the tensor of the efg, $\mathbf{V} = V_{ij}$, is symmetric, it can be diagonalized by a transformation to the principal axis system. In this coordinate system \mathbf{V} is characterized by the component with the greatest modulus V_{zz} and the asymmetry parameter

$$\eta = \frac{V_{xx} - V_{yy}}{V_{zz}}, \quad (4)$$

where the principal components have been chosen in such a way that $|V_{zz}| > |V_{yy}| > |V_{xx}|$. According to Eq. (3), V_{zz} can also be written as

$$V_{zz} = 2 \sqrt{\frac{4\pi}{5}} \int \frac{\rho(\mathbf{r})}{r^3} Y_{20}(\hat{\mathbf{r}}) d\mathbf{r}, \quad (5)$$

with the spherical harmonic $Y_{20}(\hat{\mathbf{r}})$. Equations (3) and (5) show that the spherically symmetric part of $\rho(\mathbf{r})$ does not contribute to the efg.

In order to obtain the tensor of the efg reliably we have to determine the ground-state charge density $\rho(\mathbf{r})$ with high accuracy. The appropriate tool to do this is an *ab initio* electron theory using density-functional theory and the local-density approximation. Kohn and Sham⁶ showed that the correct ground-state charge density of the system under consideration can be obtained by solving self-consistently single-particle Schrödinger equations containing an effective potential

$$[-\nabla^2 + \Phi_{\text{eff}}(\mathbf{r})]\Psi_i(\mathbf{r}) = \epsilon_i \Psi_i(\mathbf{r}) \quad (6)$$

for all N_e electrons of the system. [All formulas in the present paper are given in atomic (Rydberg) units.] The effective potential $\Phi_{\text{eff}}(\mathbf{r})$ is given by

$$\Phi_{\text{eff}}(\mathbf{r}) = - \sum_{\alpha=1}^{N_K} \frac{2Z_\alpha}{|\mathbf{r} - \mathbf{R}_\alpha|} + \int \frac{2n(\mathbf{r}')}{|\mathbf{r} - \mathbf{r}'|} d\mathbf{r}' + \Phi_{\text{xc}}(n(\mathbf{r})). \quad (7)$$

The first term is the Coulomb potential of the N_K nuclei with nuclear number Z_α at the positions \mathbf{R}_α . The second and third terms are the Hartree potential and the exchange-correlation potential, respectively. The electronic density $n(\mathbf{r})$ of the system can be obtained through

$$n(\mathbf{r}) = \sum_{i=1}^{N_e} |\Psi_i(\mathbf{r})|^2. \quad (8)$$

Equations (6)–(8) are called Kohn-Sham equations. At the end of the self-consistency cycle the ground-state charge density

$$\rho(\mathbf{r}) = \sum_{\alpha} Z_\alpha \delta(\mathbf{r} - \mathbf{R}_\alpha) - n(\mathbf{r}) \quad (9)$$

is known and the efg tensor (3) can be calculated.

There are several methods for obtaining numerical solutions of the Kohn-Sham equations [e.g., FLAPW,^{21,22} full-potential linearized-muffin-tin-orbital (FLMTO) method,²² pseudopotential method,²³ and projector augmented-wave

(PAW) method,^{24]} which differ in the choice of the basis functions for the expansion of the single-particle wave functions $\Psi_i(\mathbf{r})$. All these methods have in common that the Kohn-Sham equations are solved using the full, nonspherical effective potential only for the valence electrons. In the pseudopotential method it is assumed that the charge density of the core electrons in a solid is the same as for a free atom. This so-called frozen-core approximation leads to the fact that in a pseudopotential calculation the core-charge density is spherically symmetric and that the Kohn-Sham equations need to be solved only for the valence electrons. In the FLMTO or FLAPW method the wave functions of the true core electrons are obtained by numerical integration of Eq. (6) using only the spherically symmetric part of the effective potential. As a consequence, the core-electron density calculated by means of Eq. (8) is spherically symmetric too. Consequently, if the efg's are computed using the pseudopotential method (with subsequent reconstruction of the true valence wave functions²⁵⁾, the FLAPW, or the FLMTO method there is no contribution to the efg of the core electrons at the nucleus considered. However, due to the weighting of $\rho(\mathbf{r})$ with $1/r^3$ in Eq. (3), the efg is very sensitive to the nonspherical parts of $\rho(\mathbf{r})$ close to the nucleus. Therefore, even small deviations of the core-charge density from spherical symmetry can cause a significant change of the efg. In order to obtain reliable results for the efg from *ab initio* calculations we have to determine the core polarization, i.e., the deviation of the core-charge density from spherical sym-

metry, with high accuracy. In the following subsection first the FLAPW method, which is used throughout the present paper, will be discussed.

The FLAPW method

In the FLAPW method no shape approximations for the effective potential are made. The unit cell (or the supercell) of the solid is divided into nonoverlapping so-called muffin-tin (MT) spheres with radius R_{MT} around the nuclei and the remaining interstitial region I .²¹ In the interstitial region the wave functions of the valence electrons $\Psi_i(\mathbf{r})$ are expanded into plane waves. Inside the MT spheres the basis functions into which the $\Psi_i(\mathbf{r})$ are expanded are linear combinations of radial functions $u_l(r, E_l)$ and their energy derivatives $\dot{u}_l(r, E_l) = du_l(r, E_l)/dE_l$ multiplied by spherical harmonics $Y_{lm}(\hat{\mathbf{r}})$. $u_l(r, E_l)$ is the regular solution of the radial part of the Kohn-Sham equation (6) in the spherically averaged effective potential

$$\left[-\frac{1}{r^2} \frac{d}{dr} \left(r^2 \frac{d}{dr} \right) + \frac{l(l+1)}{r^2} + \Phi_{\text{eff}}^{\text{sph}}(r) - E_l \right] u_l(r, E_l) = 0. \quad (10)$$

The linearization energy E_l is usually set to a value near the center of the band with angular momentum l .

The basis functions in the FLAPW method are thus plane waves, which are augmented inside the MT spheres

$$\varphi^{\mathbf{k}+\mathbf{G}}(\mathbf{r}) = \begin{cases} \frac{1}{\sqrt{\Omega}} e^{i(\mathbf{k}+\mathbf{G})\mathbf{r}} & \text{for } \mathbf{r} \in I \\ \sum_{\alpha lm} [A_{\alpha lm}^{\mathbf{k}+\mathbf{G}} u_l^\alpha(r_\alpha, E_l^\alpha) + B_{\alpha lm}^{\mathbf{k}+\mathbf{G}} \dot{u}_l^\alpha(r_\alpha, E_l^\alpha)] Y_{lm}(\hat{\mathbf{r}}_\alpha) & \text{for } \mathbf{r} \in S_{\text{MT}_\alpha}^\alpha \end{cases} \quad (11)$$

In Eq. (11) \mathbf{k} is a vector of the first Brillouin zone, \mathbf{G} is a reciprocal lattice vector, Ω is the volume of the unit cell (or the supercell), S_{MT} is the muffin-tin sphere, and $\mathbf{r}_\alpha = \mathbf{r} - \mathbf{R}_\alpha$, where \mathbf{R}_α is the position of the α th nucleus. The coefficients $A_{\alpha lm}^{\mathbf{k}+\mathbf{G}}$ and $B_{\alpha lm}^{\mathbf{k}+\mathbf{G}}$ follow from the requirement that the value and slope of $\varphi^{\mathbf{k}+\mathbf{G}}(\mathbf{r})$ match on the MT sphere boundaries. They are given by

$$A_{\alpha lm}^{\mathbf{k}+\mathbf{G}} = \frac{1}{\sqrt{\Omega}} 4\pi i^l (R_{\text{MT}}^\alpha)^2 e^{i(\mathbf{k}+\mathbf{G})\mathbf{R}_\alpha} a_l^\alpha(\mathbf{k}+\mathbf{G}) Y_{lm}^*(\widehat{\mathbf{k}+\mathbf{G}}), \quad (12)$$

$$B_{\alpha lm}^{\mathbf{k}+\mathbf{G}} = \frac{1}{\sqrt{\Omega}} 4\pi i^l (R_{\text{MT}}^\alpha)^2 e^{i(\mathbf{k}+\mathbf{G})\mathbf{R}_\alpha} b_l^\alpha(\mathbf{k}+\mathbf{G}) Y_{lm}^*(\widehat{\mathbf{k}+\mathbf{G}}), \quad (13)$$

with

$$a_l^\alpha(\mathbf{k}+\mathbf{G}) = |\mathbf{k}+\mathbf{G}| j_l'(|\mathbf{k}+\mathbf{G}| R_{\text{MT}}^\alpha) \dot{u}_l^\alpha(R_{\text{MT}}^\alpha, E_l^\alpha) - j_l(|\mathbf{k}+\mathbf{G}| R_{\text{MT}}^\alpha) \dot{u}_l^{\alpha'}(R_{\text{MT}}^\alpha, E_l^\alpha), \quad (14)$$

$$b_l^\alpha(\mathbf{k}+\mathbf{G}) = j_l(|\mathbf{k}+\mathbf{G}| R_{\text{MT}}^\alpha) u_l^{\alpha'}(R_{\text{MT}}^\alpha, E_l^\alpha) - |\mathbf{k}+\mathbf{G}| j_l'(|\mathbf{k}+\mathbf{G}| R_{\text{MT}}^\alpha) u_l^\alpha(R_{\text{MT}}^\alpha, E_l^\alpha). \quad (15)$$

Here the prime stands for d/dr and the j_l are spherical Bessel functions.

Finally, the wave functions of the valence electrons are given by the expansion

$$\Psi_i^{\mathbf{k}}(\mathbf{r}) = \sum_{\mathbf{G}} C_{\mathbf{G}}^{i\mathbf{k}} \varphi^{\mathbf{k}+\mathbf{G}}(\mathbf{r}), \quad (16)$$

where reciprocal lattice vectors with $|\mathbf{k}+\mathbf{G}| < G_c$ are considered. G_c is the plane-wave cutoff. Inserting Eq. (16) in Eq. (6) yields an eigenvalue problem for the expansion coefficients $C_{\mathbf{G}}^{i\mathbf{k}}$. Once they are known, the density of the valence electrons $n^{\text{val}}(\mathbf{r})$ can be calculated using Eq. (8)

As mentioned earlier, the wave functions of the core electrons are computed in the spherically averaged effective potential. It is assumed that they are completely localized within the MT spheres. Under these assumptions, the nu-

merical solution of the radial part of the Kohn-Sham equation yields the core wave functions

$$\Psi_{lm}^{\text{core}}(\mathbf{r}_\alpha) = u_l^{\text{core}}(r_\alpha, E_l^{\text{core}}) Y_{lm}(\hat{\mathbf{r}}_\alpha) \quad (17)$$

and with the help of Eq. (8) the spherically symmetric core density $n^{\text{core}}(r_\alpha)$ of the α th nucleus.

The total charge density reads

$$\rho(\mathbf{r}) = \sum_\alpha Z_\alpha \delta(\mathbf{r} - \mathbf{R}_\alpha) - n^{\text{val}}(\mathbf{r}) - \sum_\alpha n^{\text{core}}(r_\alpha). \quad (18)$$

At the end of the self-consistency cycle of the FLAPW method we can compute the efg $V_{zz}^{\text{sph core}}$ by inserting Eq. (18) into Eq. (3). The index ‘‘sph core’’ indicates that there is, due to the spherical symmetry of the core-charge density, no contribution of the core electrons to the efg at the nuclear site.

In the FLAPW method there are two methods to abandon the spherical approximation for the core states in order to account, at least approximately, for the polarization of the highest core states. As mentioned in the Introduction, the actual spatial overlap of these core orbitals between neighboring atoms is small, but numerically significant, so they may be treated as band states. The two methods are (i) semicore calculations and (ii) local orbitals.

(i) In a FLAPW semicore calculation^{19,26} the highest core states (e.g., $3s$ and $3p$ in Cu) are treated in exactly the same way as the valence electrons, but in a separate energy window. This is done by choosing as linearization energies E_l the centers of the bands with angular momentum l of these core states. Two separate calculations are then performed for the semicore and valence electrons. At the end of an iteration step the total charge density is given by

$$\rho(\mathbf{r}) = \sum_\alpha Z_\alpha \delta(\mathbf{r} - \mathbf{R}_\alpha) - n^{\text{val}}(\mathbf{r}) - n^{\text{sc}}(\mathbf{r}) - \sum_\alpha n^{\text{core}}(r_\alpha), \quad (19)$$

where $n^{\text{core}}(r_\alpha)$ is now the density of the remaining core states of the nucleus in the α th MT sphere. Since $n^{\text{sc}}(\mathbf{r})$ is calculated using the total nonspherical effective potential (as for the valence electrons), the contribution of the semicore states to the total charge density is not spherically symmetric around the nuclear sites; hence the semicore electrons contribute to the efg.

(ii) With the help of local orbitals^{19,20} the highest core states can be treated together with the valence states in one energy window. Local orbitals are an extension of the FLAPW basis set. They are given by

$$\begin{aligned} \varphi_{lm}^{\text{LO}}(\mathbf{r}) = & [A_{lm} u_l(r, E_l^{\text{val}}) + B_{lm} \dot{u}_l(r, E_l^{\text{val}}) \\ & + C_{lm} u_l(r, E_l^{\text{HC}})] Y_{lm}(\hat{\mathbf{r}}), \end{aligned} \quad (20)$$

where the radial functions u_l are solutions of Eq. (10) and E_l^{val} is the linearization energy of the valence states with angular momentum l and E_l^{HL} that of the highest core states. The coefficients A_{lm} , B_{lm} , and C_{lm} are determined by the requirement that $\varphi_{lm}^{\text{LO}}(\mathbf{r})$ is normalized and has zero value and slope at the boundary of the MT sphere. The wave functions of the valence electrons and the highest core states are now expanded into the basis functions (11) and (20) and the

Kohn-Sham equations are solved using the full nonspherical effective potential. As in the case of semicore calculations, the charge density of the highest core states is no longer spherically symmetric; hence the influence of these states on the efg at the nuclear site is taken into account. Local orbitals are superior to semicore calculations for several reasons.¹⁹ The most important is the fact that the highest core electrons are treated in the same energy window as the valence electrons. Hence their wave functions are orthogonal to each other and there can be hybridizations between core and valence electrons.

We will discuss the accuracy of these two methods—semicore calculations and the use of local orbitals—concerning the computation of the core contribution to the efg in Sec. IV.

III. DETERMINATION OF THE CORE CONTRIBUTION TO THE efg

As we have seen in the preceding section, the wave functions of the true core electrons are calculated considering only the spherically symmetric part $\Phi_{\text{eff}}^{\text{sph}}(r)$ of the effective potential. Hence we may regard

$$\mathcal{H}^0 \psi^0 = E^0 \psi^0, \quad (21)$$

with $\mathcal{H}^0 = -\nabla^2 + \Phi_{\text{eff}}^{\text{sph}}(r)$, as the unperturbed Schrödinger equation for the core wave functions ψ^0 . In a solid we have to take into account two perturbations of the core electrons. The first perturbation is the nonspherical part of the effective potential, which we will call $\Phi^{\text{ns}}(\mathbf{r})$ in the following. If the nuclear spin I is larger than $\frac{1}{2}$, the second perturbation $\Phi^Q(\mathbf{r})$ is caused by the electric-quadrupole moment of the nucleus. Therefore we have to solve the perturbed problem

$$\underbrace{(\mathcal{H}^0 + \Phi^{\text{ns}} + \Phi^Q)}_{\mathcal{H}} \psi = E \psi. \quad (22)$$

In the following we denote the first-order perturbation of the core wave functions by $\Phi^{\text{ns}}(\Phi^Q)$ with $\psi^{\text{ns}}(\psi^Q)$, with

$$(\mathcal{H}^0 - E^0) \psi_1^{\text{ns}} = -(\Phi^{\text{ns}} - E_1^{\text{ns}}) \psi^0 \quad (23)$$

and

$$(\mathcal{H}^0 - E^0) \psi_1^Q = -(\Phi^Q - E_1^Q) \psi^0, \quad (24)$$

as can be seen by inserting $\psi = \psi^0 + \psi_1^{\text{ns}} + \psi_1^Q$ into Eq. (22) and using $E_1^{\text{ns}/Q} = \langle \psi^0 | \Phi^{\text{ns}/Q} | \psi^0 \rangle$. It becomes clear from Eqs. (23) and (24) that in first order of perturbation theory the correction ψ^{ns} is independent of the correction ψ^Q and vice versa. Physically speaking, this means that for instance, the nuclear quadrupole moment induces a polarization of the core states that is rigidly corotated when changing the orientation of the nuclear quadrupole moment. The energy of the system up to second order is given by

$$E = \frac{\langle \psi^0 + \psi_1^{\text{ns}} + \psi_1^Q | \mathcal{H} | \psi^0 + \psi_1^{\text{ns}} + \psi_1^Q \rangle}{\langle \psi^0 + \psi_1^{\text{ns}} + \psi_1^Q | \psi^0 + \psi_1^{\text{ns}} + \psi_1^Q \rangle}. \quad (25)$$

It can be shown²⁷ that the part of the second-order energy correction that depends on the orientation of the nuclear quadrupole moment relative to the nonspherical parts of the

effective potential and hence contributes to the quadrupolar interaction energy is given by (the first-order terms do not depend on this orientation)

$$E_2^{\text{ns}Q} = 2\langle \psi^0 | \Phi^Q | \psi_1^{\text{ns}} \rangle + 2\langle \psi^0 | \Phi^{\text{ns}} | \psi_1^Q \rangle + 2\langle \psi_1^{\text{ns}} | \mathcal{H}^0 - E^0 | \psi_1^Q \rangle. \quad (26)$$

The first term on the right-hand side of Eq. (26) is the orientation-dependent part of the interaction energy $\langle \psi^0 + \psi_1^{\text{ns}} | \Phi^Q | \psi^0 + \psi_1^{\text{ns}} \rangle$ of the nuclear quadrupole moment with the ‘‘external’’ efg that would arise if there were no polarization of the core states by the nuclear quadrupole moment. In reality, however, there is such a core polarization, which interacts with the external efg of the crystal, and the orientation-dependent part of the corresponding interaction energy $\langle \psi^0 + \psi_1^Q | \Phi^{\text{ns}} | \psi^0 + \psi_1^Q \rangle$ is given by the second term. The third term describes the orientation-dependent part of the polarization energy that is required to distort the originally spherically symmetric core-charge density by Φ^{ns} and Φ^Q . This is hard to see directly from the matrix element as it appears, but it becomes obvious when taking into account that the terms of the total energy E as given by Eq. (25) must describe either the energy required to generate the polarizations $|\psi_1^{\text{ns}}\rangle$ and $|\psi_1^Q\rangle$ or the interaction energies related to the existence of these polarizations. Because the latter contributions are accounted for by the first and second terms, the third term on the right-hand side of Eq. (26) has to describe (the orientation-dependent) part of the polarization energy.

Multiplying Eq. (23) by ψ^Q , Eq. (24) by ψ^{ns} , and integrating over $d\mathbf{r}$ gives us

$$\langle \psi^0 | \Phi^Q | \psi_1^{\text{ns}} \rangle = \langle \psi^0 | \Phi^{\text{ns}} | \psi_1^Q \rangle = -\langle \psi_1^{\text{ns}} | \mathcal{H}^0 - E^0 | \psi_1^Q \rangle \quad (27)$$

if we demand that $\langle \psi^0 | \psi_1^{\text{ns}} \rangle = \langle \psi^0 | \psi_1^Q \rangle = 0$ [since ψ_1^{ns} and ψ_1^Q are solutions of the inhomogeneous differential equations (23) and (24) it is always possible to orthogonalize them on ψ^0]. With the help of Eq. (27) we can simplify $E_2^{\text{ns}Q}$ to

$$E_2^{\text{ns}Q} = 2\langle \psi^0 | \Phi^Q | \psi_1^{\text{ns}} \rangle = 2\langle \psi^0 | \Phi^{\text{ns}} | \psi_1^Q \rangle. \quad (28)$$

This shows that the two orientation-dependent contributions to the interaction energy are of equal size and that either of the two contributions is exactly canceled by the polarization energy of the core charge. The important result is that we obtain the correct quadrupole interaction energy by considering either Φ^{ns} or Φ^Q as a perturbation of the core electrons (see also Refs. 1 and 28). It should be recalled that the total core polarization is of course given by the sum of $|\psi_1^{\text{ns}}\rangle$ and $|\psi_1^Q\rangle$. Nevertheless, because of the cancellation of the third term of Eq. (26) with either the first or the second term we must account for only one of the two perturbations Φ^{ns} and Φ^Q when evaluating the electric-field gradient for the calculation of the quadrupolar interaction energy.

A. Treating Φ^Q as a perturbation (Sternheimer approach)

In this subsection we will consider the potential of the nuclear quadrupole moment

$$\Phi^Q(\mathbf{r}) = \frac{C_2}{r^3} Y_{20}(\hat{\mathbf{r}}), \quad (29)$$

with the abbreviation $C_2 = -Q\sqrt{4\pi/5}$, as a perturbation of the core electrons. The problem is to find the solution of the inhomogeneous differential equation (24). The unperturbed core wave functions can be written as

$$\psi_{nlm}^0 = \frac{u_{nl}^0(r)}{r} Y_{lm}(\hat{\mathbf{r}}), \quad (30)$$

where n is the principal quantum number and l, m the quantum numbers of the angular momentum. The ψ_{nlm}^0 are degenerate with respect to the magnetic quantum number m since the energy E_{nl}^0 does not depend on m . Nevertheless, we can apply nondegenerate perturbation theory because the matrix elements of Φ^Q in the degenerate subspace

$$\langle \psi_{nlm}^0 | \Phi^Q | \psi_{nlm'}^0 \rangle = C_2 G(l2l, m0m') \int_0^\infty \frac{[u_{nl}^0(r)]^2}{r^3} dr \quad (31)$$

are zero for $m' \neq m$. The reason for this is that the Gaunt coefficients $G(l'LL, m'Mm)$, defined by

$$G(l'LL, m'Mm) = \int Y_{l'm'}^*(\hat{\mathbf{r}}) Y_{LM}(\hat{\mathbf{r}}) Y_{lm}(\hat{\mathbf{r}}) d\mathbf{O}, \quad (32)$$

vanish for $m' \neq M + m$. [Note that if the perturbation is proportional to $Y_{LM}(\hat{\mathbf{r}})$ with $M \neq 0$, the matrix of the perturbation potential in a degenerate subspace is not diagonal, so that in this case nondegenerate perturbation theory cannot be applied.]

Inserting Eq. (30) into Eq. (24) yields, for the right-hand side,

$$\begin{aligned} -(\Phi^Q - E_1^Q) \psi_{nlm}^0 &= -\sum_{l'} C_2 \left(\frac{u_{nl}^0(r)}{r^4} - \frac{u_{nl}^0(r)}{r} \right. \\ &\quad \times \left. \int \frac{[u_{nl}^0(r)]^2}{r^3} dr \delta_{ll'} \right) G(l'2l, m0m) \\ &\quad \times Y_{l'm}(\hat{\mathbf{r}}), \end{aligned} \quad (33)$$

where we used the relation

$$Y_{20}(\hat{\mathbf{r}}) Y_{lm}(\hat{\mathbf{r}}) = \sum_{l'} G(l'2l, m0m) Y_{l'm}(\hat{\mathbf{r}}). \quad (34)$$

Making for ψ_1^Q the ansatz

$$\psi_{nlm}^Q = C_2 \sum_{l'} G(l'2l, m0m) \frac{u^1(nl, l')}{r} Y_{l'm}(\hat{\mathbf{r}}), \quad (35)$$

we see that the angular-dependent parts of the left-hand and right-hand sides of Eq. (24) [the latter is given in Eq. (33)] have the same form. Comparing the different l' terms in the sum, we arrive at the inhomogeneous radial differential equation

$$\begin{aligned} &\left(-\frac{d^2}{dr^2} + \Phi_{\text{eff}}^{\text{sph}}(r) + \frac{l'(l'+1)}{r^2} - E_{nl}^0 \right) u^1(nl, l') \\ &= \left(\int \frac{[u_{nl}^0(r)]^2}{r^3} dr \delta_{ll'} - \frac{1}{r^3} \right) u_{nl}^0(r) \end{aligned} \quad (36)$$

for $u^1(nl, l')$, which can be solved numerically. For a given angular momentum of the unperturbed wave function l only certain values of l' are allowed, due to the selection rules for Gaunt coefficients. These are given by $l' = l, l \pm 2$. (For $l = 0$ only $l' = 2$ is allowed: the triangle rule.) This means that an unperturbed s state gets under the influence of Φ^Q an admixture of d character, an unperturbed p state gets admixtures of p and f character, and so on.

The first-order change of the core-electron density

$$n^1(\mathbf{r}) = 2 \operatorname{Re} \left(\sum_{nlm} \psi_{nlm}^{0*} \psi_{nlm}^Q \right) \quad (37)$$

can be written as²⁹

$$n^1(\mathbf{r}) = \frac{5}{4\pi} C_2 \frac{1}{r^2} U(r) Y_{20}(\hat{\mathbf{r}}), \quad (38)$$

with

$$U(r) = \sum_{n,l} \sum_{l'} \frac{4}{25} \sqrt{20\pi(2l+1)(2l'+1)} \\ \times G(2ll', 000) u_{nl}^0 u^1(nl, l'). \quad (39)$$

Equation (38) shows that perturbations proportional to $Y_{20}(\hat{\mathbf{r}})$ can only induce $L=2, M=0$ components in the core-electron density.

With the help of Poisson's equation, the induced potential can be computed, giving us

$$\Phi^{\text{ind}}(\mathbf{r}) = 2C_2 \left[\frac{1}{r^3} \int_0^r U(r') r'^2 dr' \right. \\ \left. + r^2 \int_r^\infty \frac{U(r')}{r'^3} dr' \right] Y_{20}(\hat{\mathbf{r}}). \quad (40)$$

By comparing Eq. (40) with Eq. (29), we may interpret $\Phi^{\text{ind}}(\mathbf{r})$ as the potential of an induced quadrupole moment

$$\Phi^{\text{ind}}(\mathbf{r}) = - \frac{Q^{\text{ind}}(r)}{r^3} \sqrt{\frac{4\pi}{5}} Y_{20}(\hat{\mathbf{r}}), \quad (41)$$

with

$$Q^{\text{ind}}(r) = 2Q \left[\int_0^r U(r') r'^2 dr' + r^5 \int_r^\infty \frac{U(r')}{r'^3} dr' \right]. \quad (42)$$

The total quadrupole moment of the system nucleus plus core electrons is therefore given by

$$Q^{\text{tot}}(r) = Q + Q^{\text{ind}}(r) = Q[1 - \gamma(r)], \quad (43)$$

where we introduced the Sternheimer function

$$\gamma(r) = -2 \left[\int_0^r U(r') r'^2 dr' + r^5 \int_r^\infty \frac{U(r')}{r'^3} dr' \right]. \quad (44)$$

The limit of $\gamma(r)$ for $r \rightarrow \infty$ is the well-known Sternheimer factor γ_∞ .

An external point charge (external to the system nucleus plus core electrons, e.g., a valence electron or a neighboring nucleus) then interacts with the local quadrupole moment

$Q^{\text{tot}}(r) = Q[1 - \gamma(r)]$. From a mean-field-like viewpoint the influence of the core electrons on the quadrupolar interaction energy can therefore be accounted for by weighting the external charges in the formula for the computation of the efg (3) with the factor $[1 - \gamma(r)]$. If $\rho(\mathbf{r})$ is the total charge density of the system, calculated with spherically symmetric core states, the ‘‘effective’’ efg at the nucleus under consideration is thus given by

$$V_{ij} = \int [1 - \gamma(r)] \rho(\mathbf{r}) \left(\frac{3x_i x_j}{r^5} - \frac{\delta_{ij}}{r^3} \right) d\mathbf{r}. \quad (45)$$

In Eq. (45) we can use the total charge density of the system instead of the charge density of the external charges because the spherically symmetric core-charge density of the nucleus considered does not contribute to V_{ij} . In this context ‘‘effective’’ means that we obtain, using V_{ij} from Eq. (45), the correct quadrupolar interaction energy with the nuclear quadrupole moment Q and consequently the correct quadrupolar splitting of the nuclear levels, which is proportional to QV_{zz} .

These considerations show that in this method the core contribution to the efg at the nucleus is given by

$$V_{ij}^{\text{core}} = - \int \gamma(r) \rho(\mathbf{r}) \left(\frac{3x_i x_j}{r^5} - \frac{\delta_{ij}}{r^3} \right) d\mathbf{r}, \quad (46)$$

where $\rho(\mathbf{r})$ is again the total charge density of the system, calculated with spherically symmetric core states, and $\gamma(r)$ is the Sternheimer function, calculated in the spherically symmetric part of the effective potential. The total efg is finally given by

$$V_{ij} = V_{ij}^{\text{sph core}} + V_{ij}^{\text{core}}, \quad (47)$$

where $V_{ij}^{\text{sph core}}$ is the result of a calculation with spherically symmetric core-charge density.

B. Treating Φ^{ns} as a perturbation (effective-potential method)

This second but equivalent method (see above) considers the nonspherical part of the effective potential

$$\Phi^{\text{ns}}(\mathbf{r}) = \sum_{L \neq 0, M} \Phi_{LM}^{\text{ns}}(r) Y_{LM}(\hat{\mathbf{r}}), \quad (48)$$

as a perturbation of the core electrons. In principle, we can calculate the perturbation of the core wave functions ψ_{nl}^{ns} by solving Eq. (23). However, the method described in Sec. III A can only be applied if Φ^{ns} has only components with $M=0$. This is due to the fact that in the m -degenerate subspace of the unperturbed states ψ_{nlm}^0 the matrix of the perturbation

$$\langle \psi_{nlm}^0 | \Phi^{\text{ns}} | \psi_{nlm'}^0 \rangle = \sum_{L \neq 0, M} G(1Ll, mMm') \\ \times \int_0^\infty \Phi_{LM}^{\text{ns}}(r) [u_{nl}^0(r)]^2 dr \quad (49)$$

is not diagonal for $M \neq 0$ since the Gaunt coefficients do not vanish if the relation $m = M + m'$ is satisfied.

In the following we will present an alternative approach to find the core wave functions in the full nonspherical effective potential. Instead of the first-order perturbation equation (23) we solve

$$\left(-\nabla^2 + \Phi_{\text{eff}}^{\text{sph}}(r) + \sum_{L \neq 0, M} \Phi_{LM}^{\text{ns}}(r) Y_{LM}(\hat{\mathbf{r}}) \right) \psi_i(\mathbf{r}) = E \psi_i(\mathbf{r}). \quad (50)$$

This can be done by expanding the $\psi_i(\mathbf{r})$ ($i=1, \dots, N_{\text{CE}}$, where N_{CE} is the number of core electrons) in a suitable chosen set of basis functions. In our approach the expansion is given by

$$\psi_i(\mathbf{r}) = \sum_{lm} C_{lm} \frac{u_l^0(r)}{r} Y_{lm}(\hat{\mathbf{r}}) + \sum_{lma} D_{lm}^a r^l \exp(-ar^2) Y_{lm}(\hat{\mathbf{r}}). \quad (51)$$

$\psi_{nlm}^0 = u_l^0(r)/r Y_{lm}(\hat{\mathbf{r}})$ are the unperturbed core wave functions, which means the first $N_{\text{CE}}/2$ solutions of Eq. (50) if we consider only the spherically averaged effective potential. The second part of the basis set, which is necessary since the perturbation of the core wave functions cannot be described by the ψ_{nlm}^0 alone, is given by Gaussians. In this part we considered values of l up to 4. For the width of these Gaussians a we choose ten different values between zero and the MT sphere radius. The convergence of the results with respect to the number and choice of the a can be monitored by comparing them with the results of the previous method for cases with $M=0$, where we have to solve an inhomogeneous differential equation and where no additional basis functions are needed. We find that using ten different values gives, to a very good approximation, the same perturbed wave functions and hence the same core contributions to the efg.

Inserting Eq. (51) into Eq. (50), we obtain an eigenvalue problem for the coefficients C_{lm} and D_{lm}^a , which can be solved numerically. The nonspherical core-electron density is finally given by

$$n^{\text{core}}(\mathbf{r}) = \sum_i |\psi_i(\mathbf{r})|^2 \quad (52)$$

and the core contribution to the efg can be calculated with the help of

$$V_{ij} = - \int n^{\text{core}}(\mathbf{r}) \left(\frac{3x_i x_j}{r^5} - \frac{\delta_{ij}}{r^3} \right) d\mathbf{r}. \quad (53)$$

In principle, it is possible to include the calculation of the nonspherical core-charge density in the self-consistency cycle of the FLAPW method. This can be done by computing the contribution of the core-charge density to the nonspherical components of the effective potential in each iteration by means of Poisson's equation. However, in general, this contribution is small compared to the one of the valence electrons. Therefore, the reaction of the valence electrons on the nonspherical core contribution to the effective potential is negligible, as we have shown by several test calculations, and it suffices to compute the nonspherical core-charge density once at the end of the self-consistency cycle.

TABLE I. Decomposition of the core contribution to the efg at the NN site of a substitutional Ni atom in Cu.

State	V_{zz}^{core} in 10^{19} V/m ²
1s	-0.2
2s	0.0
2p	-1.6
3s	0.1
3p	-7.2
1s-3p	-8.9

IV. RESULTS

A. efg near a substitutional Ni or Pd atom in Cu

In order to test the accuracy of the different methods to determine the core contribution to the efg (e.g., FLAPW semicore calculations or calculations with local orbitals, and the effective-potential approach) we have calculated the efg at the nearest-neighbor (NN) site of substitutional Be, Ni, Pd, and Pt atoms in Cu using a supercell containing 15 Cu atoms and one substitutional atom. As a representative example to demonstrate the effects we discuss the results for the system Ni in Cu because it gives a rather large core contribution to the efg. Furthermore, the experimental value for the efg at the NN site is accurately known from nuclear quadrupole double-resonance measurements on dilute CuNi alloys.³⁰ It is given by $|V_{zz}^{\text{expt}}| = 42 \times 10^{19}$ V/m².

Using the FLAPW method and treating the 1s-3p electrons of Cu and Ni as spherically symmetric core states, we obtained at the NN Cu atom $V_{zz} = -36.1 \times 10^{19}$ V/m². In this calculation we have used eight \mathbf{k} points according to Chadi and Cohen,³¹ Gaussian broadening,³² a plane-wave cutoff of $G_c = 4.0$ a.u.⁻¹, and the experimental lattice constant $a_0 = 6.82$ a.u. and we took into account the relaxation of the Cu atoms surrounding the Ni atom.

Applying the effective-potential method at the end of the FLAPW self-consistency cycle leads to a core contribution to the efg of $V_{zz}^{\text{core}} = -8.9 \times 10^{19}$ V/m². This gives us the theoretical value $V_{zz} = -44.9 \times 10^{19}$ V/m², in reasonable agreement with the experimental value. (For a detailed comparison between theory and experiment we have to use more \mathbf{k} points as well as larger supercells in order to avoid ‘‘finite-size’’ effects.) The core contribution to the efg can be decomposed into the contributions of the different core states. Table I shows that the main contribution comes from the 3p electrons. The contribution of the 2p electrons is small and that of s electrons can be neglected.

In Sec. III A we have already seen that within the framework of a first-order perturbation approach a $L=2$, $M=0$ perturbation can only induce a $L=2$, $M=0$ component in the core-charge density. Similarly, it can be shown that perturbations proportional to Y_{LM} induce to first order only L components in the core-charge density. Because for the efg only the $L=2$ components are relevant, only perturbations with $L=2$ must be considered to determine the core contribution to the efg. The principal axis system of the total efg tensor as well as of $V_{ij}^{\text{sph core}}$ and V_{ij}^{core} at the NN site of the Ni atom is given by $\hat{x} = (0, 0, -1)$, $\hat{y} = (-1/\sqrt{2}, 1/\sqrt{2}, 0)$, and $\hat{z} = (1/\sqrt{2}, 1/\sqrt{2}, 0)$. In this coordinate system only the two $L=2$ components Φ_{20}^{ns} and Φ_{22}^{ns} of the effective potential are allowed by

TABLE II. Decomposition of the $3p$ contribution to the efg at the NN site of a substitutional Ni atom in Cu into contributions from radial and angular excitations.

$3p$ excitation	V_{zz}^{core} in 10^{19} V/m 2
Radial	-7.4
Angular	+0.2

symmetry at the NN site of the Ni atom and the principal component of the core contribution to the efg, V_{zz}^{core} , is, according to Eq. (5), determined by the $L=2, M=0$ component of the core-charge density induced by $\Phi_{20}^{\text{ns}}Y_{20}$ (see above). For the determination of V_{zz}^{core} we therefore have to consider only the perturbation $\Phi_{20}^{\text{ns}}Y_{20}$ and consequently we can calculate the perturbation of the core wave functions ψ_1^{ns} by solving Eq. (23) with the method described in Sec. III A (we have only to replace Φ^Q by $\Phi_{20}^{\text{ns}}Y_{20}$) since the matrix representation of $\Phi_{20}^{\text{ns}}Y_{20}$ in an m -degenerate subspace is diagonal. In Sec. III A we have shown that a perturbation, which is proportional to $Y_{20}(\hat{\mathbf{r}})$, adds wave functions with $l'=2$ to an unperturbed s state and with $l'=l, l\pm 2$ to unperturbed states of angular momentum $l\neq 0$. An unperturbed s (p) state gets under the influence of $\Phi_{20}^{\text{ns}}Y_{20}$ an admixture of d (p and f) character. According to Sternheimer, admixtures that have the same angular momentum l as the unperturbed state are called radial excitations (for example, in the case of a $p\rightarrow p$ excitation), whereas those with $l'=l\pm 2$ are called angular excitations. The contribution of the $3p$ electrons to the efg can be further decomposed into these radial and angular excitations (Table II). It turns out that the contribution of angular excitations ($p\rightarrow f$) is very small.

The contribution of the $3s$ and $3p$ electrons of Cu to the efg at the NN site of a substitutional Ni atom can, in principle, also be calculated with a FLAPW semicore calculation or with the help of local orbitals (see Sec. II A), whereas the contributions of the states $1s$ - $2p$ that add up to -1.8×10^{19} V/m 2 (Table I) cannot be obtained by these methods. The calculation in which the Cu $3p$ states are treated using local orbitals (the remaining core states $1s$ - $3s$ are still treated as spherically symmetric states) gives us a contribution of the $3p$ electrons to the efg of $V_{zz}^{3p}=-6.7\times 10^{19}$ V/m 2 , in satisfying agreement with the result of the effective-potential method (-7.2×10^{19} V/m 2).

Treating the $3s$ and $3p$ electrons by means of a semicore calculation, we obtain $V_{zz}^{3p}=-0.4\times 10^{19}$ V/m 2 , which is much too small compared to the results of the effective-potential method and the local-orbital calculation. We will now discuss the reason for the failure of the semicore calculation.

If we choose the principal axis system of the efg as our coordinate system, V_{zz}^{3p} is dominated by the radial excitation of the $3p$ electrons under the influence of the $L=2, M=0$ component of the effective potential, $\Phi_{20}^{\text{ns}}Y_{20}$. Figure 1 shows the radial part of the $3p$ radial excitation, induced by $\Phi_{20}^{\text{ns}}Y_{20}$ and calculated by solving Eq. (23) with the method described in Sec. III A. In a semicore calculation the basis functions with p character inside the MT sphere of the nucleus considered are given by

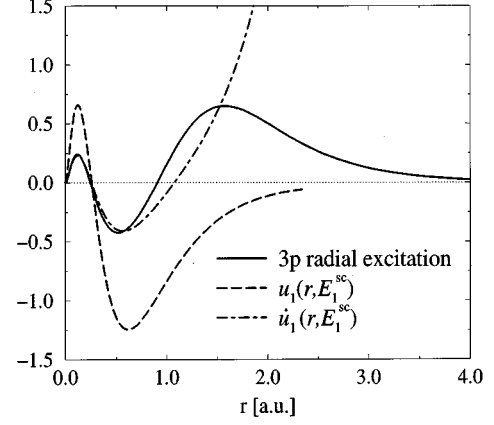


FIG. 1. Radial excitation ($p\rightarrow p$) of the $3p$ state, induced by $\Phi_{20}^{\text{ns}}Y_{20}$ and multiplied by 5000. Also shown are the $3p$ -like augmentation function $u_1(r, E_1^{\text{sc}})$ and its energy derivative. The radius of the MT sphere is 2.3 a.u.

$$\varphi_{3p}^{\mathbf{k}+\mathbf{G}}(\mathbf{r}) = \sum_m [A_{1m}^{\mathbf{k}+\mathbf{G}} u_1(r, E_1^{\text{sc}}) + B_{1m}^{\mathbf{k}+\mathbf{G}} \dot{u}_1(r, E_1^{\text{sc}})] Y_{1m}(\hat{\mathbf{r}}) \quad (54)$$

[see Eq. (11)]. The function $u_1(r, E_1^{\text{sc}})$ and its energy derivative $\dot{u}_1(r, E_1^{\text{sc}})$ are also shown in Fig. 1. It is evident that in the region close to the nucleus (which is most important for the computation of the efg) the radial excitation of the $3p$ state can, in principle, be described by $\dot{u}_1(r, E_1^{\text{sc}})$. But we have to remember that the coefficients $A_{1m}^{\mathbf{k}+\mathbf{G}}$ and $B_{1m}^{\mathbf{k}+\mathbf{G}}$ in Eq. (54) are determined by the augmentation. Since the value and slope of $u_1(r, E_1^{\text{sc}})$ are very small at the MT sphere boundary, the coefficients $B_{1m}^{\mathbf{k}+\mathbf{G}}$ are, according to Eqs. (13) and (15), very small too. The $l=1$ part of the $3p$ wave function (in the following reasoning we will only consider the Γ point $\mathbf{k}=\mathbf{0}$) inside the MT sphere can be written as

$$\begin{aligned} \Psi_{3p}(\mathbf{r}) &= \sum_{\mathbf{G}} C_{\mathbf{G}}^{3p} \varphi_{3p}^{\mathbf{G}}(\mathbf{r}) \\ &= \sum_m [a_m^{3p} u_1(r, E_1^{\text{sc}}) + b_m^{3p} \dot{u}_1(r, E_1^{\text{sc}})] Y_{1m}(\hat{\mathbf{r}}), \end{aligned} \quad (55)$$

with

$$a_m^{3p} = \sum_{\mathbf{G}} C_{\mathbf{G}}^{3p} A_{1m}^{\mathbf{G}}, \quad b_m^{3p} = \sum_{\mathbf{G}} C_{\mathbf{G}}^{3p} B_{1m}^{\mathbf{G}}. \quad (56)$$

Although the coefficients $B_{1m}^{\mathbf{G}}$ are small, it may be possible that a_m^{3p} and b_m^{3p} are of comparable magnitude. However, we have to keep in mind that the $3p$ electrons of Cu are almost completely confined within the MT sphere and that therefore the value and slope of $\Psi_{3p}(\mathbf{r})$ must be very small at the MT sphere boundary. Since $\dot{u}_1(r, E_1^{\text{sc}})$ is large near this boundary, the coefficient b_m^{3p} has to be very small in order to avoid an energetically unfavorable large delocalization of the $3p$ electrons. In contrast to this, the coefficient a_m^{3p} should take a significant value in order to account for the radial excitation of the $3p$ wave function. However, the accurate account of the radial excitation is energetically much less important

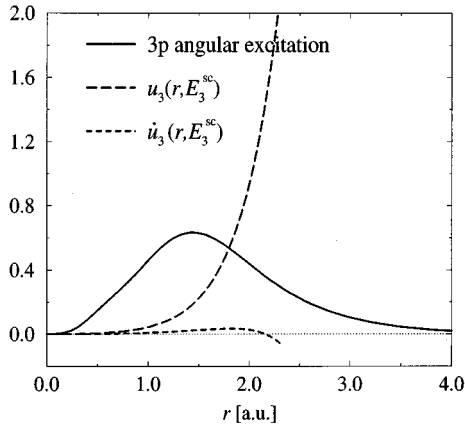


FIG. 2. Angular excitation ($p \rightarrow f$) of the $3p$ state, induced by $\Phi_{20}^{\text{ns}} Y_{20}$ and multiplied by 5000. Also shown are the augmentation function $u_3(r, E_3^{\text{sc}})$ and its energy derivative with f character. The radius of the MT sphere is 2.3 a.u.

than the accurate description of the correct localization. Furthermore, the coefficients C_G^{3p} are determined by the variation principle in such a way that $\Psi_{3p}(\mathbf{r})$ is small in the interstitial region. Under these circumstances, it is impossible, due to the limited variational freedom, that a superposition of the basis functions according to Eq. (55) yields a good description of the radial excitation in the whole MT sphere.

For the angular excitation of the $3p$ state under the influence of $\Phi_{20}^{\text{ns}} Y_{20}$ the situation is similar. Figure 2 shows the radial part of the angular excitation of the $3p$ Cu state at the NN site of a substitutional Ni atom induced by $\Phi_{20}^{\text{ns}} Y_{20}$ and again calculated by solving Eq. (23). Also shown are the augmentation functions $u_3(r, E_3^{\text{sc}})$ and $\dot{u}_3(r, E_3^{\text{sc}})$ with f character. It can be seen that the angular excitation of the $3p$ state can only poorly be described by these augmentation functions. Therefore, the contribution of angular excitations to the efg is not correctly reproduced by semicore calculations. These considerations show that we may not expect to obtain accurate values for the contribution of the highest core electrons (e.g., the $3s$ and $3p$ electrons of Cu) to the efg using a FLAPW semicore calculation since neither the important radial nor the angular excitation is described correctly.

The situation is completely different if the $3p$ state of Cu is treated with the help of local orbitals together with the valence electrons in one energy window. In this case the basis functions with p character inside the MT sphere are given by the local orbital

$$\varphi_{1m}^{\text{LO}}(\mathbf{r}) = [A_{1m} u_1(r, E_1^{\text{val}}) + B_{1m} \dot{u}_1(r, E_1^{\text{val}}) + C_{1m} u_1(r, E_1^{3p})] Y_{1m}(\hat{\mathbf{r}}) \quad (57)$$

and

$$\varphi^{\mathbf{k}+\mathbf{G}}(\mathbf{r}) = \sum_m [A_{1m}^{\mathbf{k}+\mathbf{G}} u_1(r, E_1^{\text{val}}) + B_{1m}^{\mathbf{k}+\mathbf{G}} \dot{u}_1(r, E_1^{\text{val}})] Y_{1m}(\hat{\mathbf{r}}), \quad (58)$$

where the augmentation function $u_1(r, E_1^{\text{val}})$ and its energy derivative are calculated for an energy in the valence-band

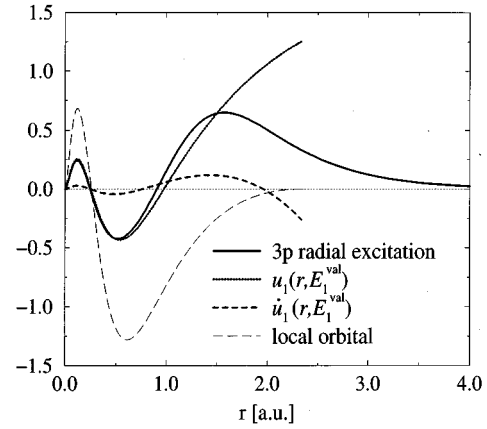


FIG. 3. Radial excitation of the $3p$ state (induced by $\Phi_{20}^{\text{ns}} Y_{20}$ and multiplied by 5000), augmentation functions $u_1(r, E_1^{\text{val}})$ and $\dot{u}_1(r, E_1^{\text{val}})$, and local orbital for the NN Cu atom of a substitutional Ni atom. The radius of the MT sphere is 2.3 a.u.

region and $u_1(r, E_1^{3p})$ for the energy of the center of the small $3p$ band. These three augmentation functions are shown in Fig. 3 together with the radial excitation ($p \rightarrow p$) of the $3p$ state induced by $\Phi_{20}^{\text{ns}} Y_{20}$. It is evident that now the radial excitation of the $3p$ state can be described by the two functions $u_1(r, E_1^{\text{val}})$ and $\dot{u}_1(r, E_1^{\text{val}})$, at least in the region close to the nucleus (see Fig. 3). The part of the $3p$ wave function with p character is now given by (again for $\mathbf{k}=\mathbf{0}$)

$$\Psi_{3p}(\mathbf{r}) = \sum_m C_m^{\text{LO}} \varphi_{1m}^{\text{LO}}(\mathbf{r}) + \sum_m [a_m^{3p} u_1(r, E_1^{\text{val}}) + b_m^{3p} \dot{u}_1(r, E_1^{\text{val}})] Y_{1m}(\hat{\mathbf{r}}). \quad (59)$$

The coefficients a_m^{3p} and b_m^{3p} are adjusted by the variation principle in such a way that, on the one hand, the value and slope of $\Psi_{3p}(\mathbf{r})$ are small but not zero at the MT radius (accounting for the small overlap of neighboring $3p$ wave functions) and that, on the other hand, the radial excitation is reproduced accurately. In contrast to the FLAPW semicore calculation there are now two functions $u_1(r, E_1^{\text{val}})$ and $\dot{u}_1(r, E_1^{\text{val}})$ that contribute with comparable weight to the wave function at the MT sphere boundary and are both able to describe the radial excitation in the region close to the nucleus. Consequently, in a FLAPW calculation with local orbitals the variational freedom is increased compared to a semicore calculation and the contribution of the radial excitation of the $3p$ state to the efg is reproduced.

Figures 1–3 also show that the radial and angular excitations of the unperturbed $3p$ wave function are very small (remember that they have been multiplied by 5000). Therefore, the orthogonality of the core wave functions, which is, for true core states, exactly fulfilled if these are treated as spherically symmetric states,²⁰ is to a very good approximation maintained.

For the angular excitation of the $3p$ state the situation that arises when using local orbitals is analogous to the case of a semicore calculation. It is not accurately reproduced in a FLAPW calculation using local orbitals.

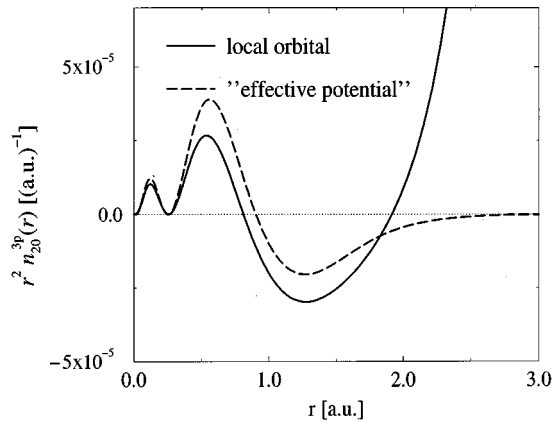


FIG. 4. $l=2, m=0$ component of the $3p$ core-electron density, multiplied by r^2 , of a NN Cu atom of substitutional Ni. The full curve is calculated using local orbitals for the $3p$ state and the dashed curve using the effective-potential method (considering only radial excitations).

Figure 4 shows the 20 component of the charge density of the $3p$ electrons multiplied with r^2 and calculated with the effective-potential method as well as with local orbitals. This component determines the contribution of the $3p$ electrons to the efg [see Eq. (53)]. We have already seen that angular excitations are not correctly described by a FLAPW calculation with local orbitals. Additionally, Fig. 2 shows that in the region close to the nucleus the augmentation functions with f character are very small; hence, in this region the contribution of angular excitations to $r^2 n_{20}^{3p}(r)$ in a FLAPW semi-core or local orbital calculation is negligibly small. Therefore, we may assume that for a comparison of the local-orbital result for $n_{20}^{3p}(r)$ with the result of the effective-potential method it is reasonable to consider in the last method only radial excitations. This assumption is justified by the reasonable agreement of the two curves in Fig. 4, especially in the important region close to the nucleus. This, together with the fact that the contribution of angular excitations is, in general, very small (Table II), results in the good agreement of the two values of V_{zz}^{3p} stated before.

In contrast, in the region near the boundary of the MT sphere there is a large discrepancy between the two results for $r^2 n_{20}^{3p}(r)$ shown in Fig. 4. This is due to the fact that the $3p$ state is treated completely different in the two methods. In the effective-potential method the $3p$ state is treated as an atomic state with no solid-state boundary conditions to be satisfied, whereas in a calculation using local orbitals it is treated as a band state. The calculation with local orbitals shows that the asphericity of the $3p$ charge density is largest at the MT sphere boundary due to the overlap of the $3p$ wave functions of neighboring atoms.

In the following we will address the question whether or not it is, concerning the computation of the efg, a good approximation to treat the $3p$ electrons of Cu as atomic states. The density of the $3p$ electrons is almost completely confined within the MT sphere, as can be seen in Fig. 5. Nevertheless, there is a small amount outside the MT sphere, which gives a direct contribution to chemical binding. In order to separate the contribution to $n_{20}^{3p}(r)$ arising from the overlap of neighboring $3p$ wave functions from the contri-

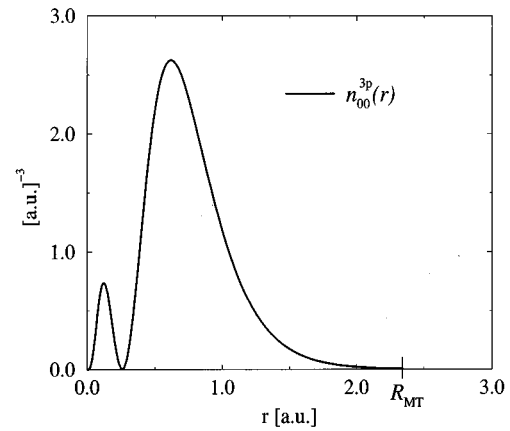


FIG. 5. $l=0, m=0$ component of the $3p$ core-electron density of a NN Cu atom of substitutional Ni. $R_{MT}=2.3$ a.u. is the radius of the MT sphere.

bution arising from the asphericity of the effective potential inside the MT sphere we performed a calculation in a MT potential, i.e., a calculation in which only the spherically symmetric part of the effective potential inside the MT sphere is considered and the potential in the interstitial region is set to zero. Figure 6 shows again the 20 component of the $3p$ charge density, multiplied by r^2 . The full line is the result of the FLAPW calculation in which the $3p$ states are treated using local orbitals and where the full nonspherical effective potential has been taken into account. This curve is the same as that plotted in Fig. 4. As already mentioned, this calculation gives $V_{zz}^{3p} = -6.7 \times 10^{19}$ V/m². At the end of the self-consistency cycle we made an additional last iteration in which only the spherically symmetric part of the effective potential inside the MT sphere was considered (the MT potential). This results in the dashed curve shown in Fig. 6. In a calculation using a MT potential the nonspherical parts of the $3p$ charge density can only be caused by the overlap of the $3p$ wave functions of neighboring atoms, i.e., by the contribution of the $3p$ states to chemical binding. This overlap leads to an increase of $n_{20}^{3p}(r)$ near the MT sphere bound-

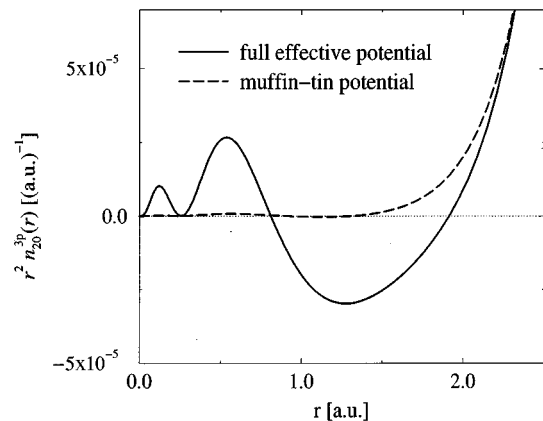


FIG. 6. 20 component of the $3p$ electron density $r^2 n_{20}^{3p}(r)$ of a NN Cu atom of substitutional Ni, calculated using local orbitals. The full curve is obtained if the full effective potential is used; the dashed curve is the result of a calculation in a MT potential. The MT radius is 2.3 a.u.

TABLE III. Quadrupolar transition frequencies of the ^{63}Cu nuclei near a substitutional Pd atom, calculated with the FLAPW method using ten Chadi-Cohen \mathbf{k} points, $G_c=3.4$ a.u. $^{-1}$, and a relaxed 64-atom supercell. The core contribution ($1s-3p$) to the efg has been calculated with the effective-potential method. 0 indicates that η vanishes by symmetry.

Shell	ν_q (kHz)	Theory		Experiment	
		η	$V_{zz}^{\text{core}}/V_{zz}^{\text{sph core}}$	ν_q (kHz)	η
1	3160	0.3	-0.07	3145	0.2
2	520	0	-0.08	534	
3	390	0.6	+0.27	241	

ary. In the region close to the nucleus, however, the values of $n \frac{3}{2} \rho(r)$ from the MT potential calculation are very small compared to the values calculated in the full effective potential. Consequently, the calculation in the MT potential gives, similar to the semicore calculation, a very small value for the $3p$ contribution to the efg, $V_{zz}^{3p} = -0.2 \times 10^{19}$ V/m 2 . V_{zz}^{3p} is thus almost completely determined by the polarization of the $3p$ state under the influence of the nonspherical part of the effective potential. From these considerations we may conclude that for the determination of the contribution of the $3p$ electrons to the efg in Cu it is a good approximation to treat them as atomic states.

The question of which of the two methods yields the most accurate results is difficult to answer. Local orbitals certainly have the advantage that they can also be applied to systems with extended core states (see the Introduction). The effective-potential method is not applicable for these systems. Points in favor of the effective-potential method are that (i) the flexibility of the basis set may be superior compared to a local orbital calculation for the case of a very small overlap of neighboring core states, where the core contribution to the efg arises nearly exclusively from the aspherical effective potential; (ii) the contribution of all core electrons to the efg can be determined; and (iii) both radial and angular excitations can be considered. Furthermore, it can be applied in combination with the pseudopotential method after the reconstruction of the true valence wave functions from the pseudovalence wave functions 25 too.

The calculations for the substitutional Ni atom in Cu reported so far have been performed with a small supercell containing 16 atoms. This supercell size allows only the determination of the efg at the NN sites of the Ni atom because the next NN already lies on the boundary of the supercell. Additionally, the calculated efg at the NN site may be influenced by the small supercell size (the finite-size effect). Hence, for a direct comparison with experiment we have to use a larger supercell. As an example we calculated the efg's near a substitutional Pd atom in Cu using a 64-atom supercell. In this supercell the atoms of the fourth shell around the impurity lie on the supercell boundary, so that we can determine the relaxed atomic positions and efg's for the first three shells. The relaxed atomic positions are in units of a_0 given by (0.5080,0.5080,0) for the first, (1.0012,0,0) for the second, and (0.4996,0.4996,1.0020) for the third shell. Table III shows the calculated transition frequencies

TABLE IV. Decomposition of the core contribution to the efg at the NN site of a substitutional Fe atom in Al.

State	V_{zz}^{core} in 10^{19} V/m 2
1s	0.8
2s	1.0
2p	-13.5
1s-2p	-11.6

$$\nu_q = \frac{eQ|V_{zz}|}{2h} \sqrt{1 + \frac{\eta^2}{3}} \quad (60)$$

and the asymmetry parameter for the Cu atoms (nuclear spin $I = \frac{3}{2}$) up to shell 3 together with experimental values for ν_q obtained with the nuclear quadrupole double resonance (NQDOR) technique 33 and for η obtained by means of NMR. 34 For the nuclear quadrupole moment of the Cu isotope ^{63}Cu we used $Q = -220 \times 10^{-31}$ m 2 . 35 Table III shows that theory and experiment agree excellently for the first two shells. Again the core contribution to the efg is considerable and improves the agreement with experiment significantly. The third shell, however, is influenced by finite-size effects, which lead to a discrepancy between theory and experiment. Calculations with a 16-atom supercell for the same system showed that already this supercell size gives reasonable values for the relaxed atomic positions of the NN atoms of the substitutional Pd atom and for the efg at the NN nuclear sites (see also Ref. 3).

B. efg near a substitutional Fe or V atom in Al

We have performed calculations of the efg near Fe or V substitutional atoms in Al. Because the core contribution to the efg is much larger for Fe than for V, we confine ourselves mainly to the discussion of the first case. As in the case of a substitutional Ni atom in Cu, the calculations of the efg at the NN site of a substitutional Fe atom in Al have been performed with a 16-atom supercell and the FLAPW method. The experimental value for the efg and the asymmetry parameter at the NN site is $|V_{zz}^{\text{expt}}| = 42 \times 10^{19}$ V/m 2 and $\eta = 0.6$. 36

A FLAPW calculation (40 \mathbf{k} points according to Chadi and Cohen, Gaussian broadening, $G_c = 3.4$ a.u. $^{-1}$, the experimental lattice constant $a_0 = 7.65$ a.u., and relaxation of the Al atoms surrounding the Fe atom are taken into account), in which the $1s-2p$ electrons of Al and the $1s-3p$ electrons of Fe are treated as spherically symmetric core states, gives, for the efg at the NN site of the Fe atom, $V_{zz} = -38.4 \times 10^{19}$ V/m 2 and an asymmetry of 0.87.

At the end of the self-consistency cycle we obtain by the effective-potential method a rather large core contribution to the efg of $V_{zz}^{\text{core}} = -11.6 \times 10^{19}$ V/m 2 . The total theoretical results for the efg, $V_{zz} = -50.0 \times 10^{19}$ V/m 2 , and for the asymmetry parameter $\eta = 0.7$ are, despite the small supercell used, in good agreement with the experimental values. The decomposition of the core contribution to the efg into the contributions of the different core states is shown in Table IV. The main contribution comes from the $2p$ electrons. Similar to the case of Cu, the contribution of s electrons can be neglected. The contribution of the $2p$ electrons to the efg

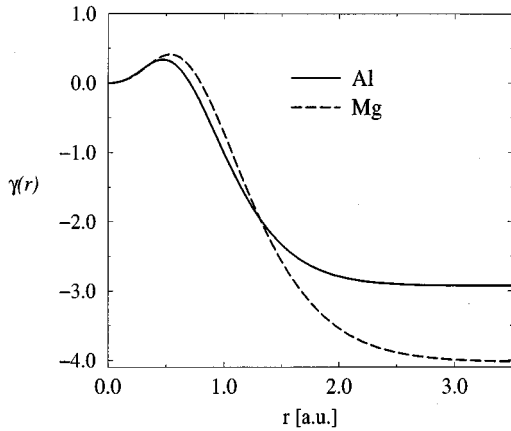


FIG. 7. Sternheimer function $\gamma(r)$ of the Al atom next to a substitutional Fe atom (solid line) and a Mg atom (dashed line) in the perfect, hexagonal lattice, calculated in the spherically symmetric part of the effective potential. The contribution of the $1s$ - $2p$ core electrons has been considered. (Al, $R_{\text{MT}}=2.61$ a.u.; Mg, $R_{\text{MT}}=2.95$ a.u.)

can be decomposed into the radial and angular excitations. The radial excitation contributes -14.8×10^{19} V/m²; the angular excitation gives only a very small contribution of 1.3×10^{19} V/m².

We have also calculated the core contribution to the efg using the Sternheimer function approach described in Sec. III A. At the end of the self-consistency cycle of the above-mentioned FLAPW calculation, in which the $1s$ - $2p$ electrons of Al are treated as spherically symmetric states, the Sternheimer function can be computed with the help of Eq. (44) using the spherically symmetric part of the effective potential in Eq. (36). For the Al atom next to the substitutional Fe atom $\gamma(r)$ is shown in Fig. 7. In the region outside the $1s$ - $2p$ charge density $\gamma(r)$ takes the constant value $\gamma_{\infty} = -2.93$. Figure 7 shows that this is the case for $r > R_{\text{MT}}$, i.e., outside the MT sphere. In order to compute the core contribution to the efg, we can therefore apply Eq. (46) for the charge density $\rho(\mathbf{r})$ inside the MT sphere [note that $\rho(\mathbf{r})$ is the charge density obtained in the FLAPW calculation with spherically symmetric $1s$ - $2p$ states] and add the contribution to the efg from outside the MT sphere of the considered Al atom multiplied with γ_{∞} . This gives $V_{zz}^{\text{core}} = -11.3 \times 10^{19}$ V/m². The total theoretical result is then $V_{zz} = -49.7 \times 10^{19}$ V/m² and $\eta = 0.69$, in excellent agreement with the result of the effective-potential method (see above). This demonstrates strikingly the equivalence of the two methods discussed in Sec. III.

A FLAPW calculation in which the $2p$ states of Al (and the $3p$ states of Fe) are treated using local orbitals gives a contribution of the $2p$ electrons to the efg of $V_{zz}^{2p} = -11.1 \times 10^{19}$ V/m², again in satisfying agreement with the result of the effective-potential method, $V_{zz}^{2p} = -13.5 \times 10^{19}$ V/m². Figure 8 shows the local orbital and effective-potential result for the 20 component of the density of the $2p$ electrons multiplied with r^2 . In the calculation using the effective-potential method we have, for the reasons discussed in Sec. IV A, again only considered radial excitations. In the region close to the nucleus both curves in Fig. 8 agree reasonably. The reason for the difference be-

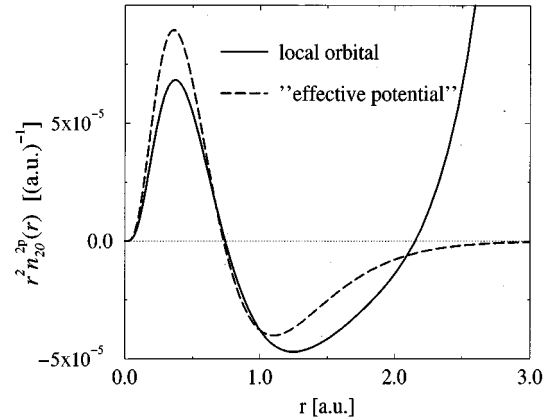


FIG. 8. $l=2$, $m=0$ component of the $2p$ core-electron density, multiplied by r^2 , of an Al atom next to a substitutional Fe atom. The full curve is calculated using local orbitals for the $2p$ state and the dashed curve using the effective-potential method (considering only radial excitations). $R_{\text{MT}}=2.61$ a.u.

tween the two curves in the region near the boundary of the MT sphere is the same as discussed in Sec. IV A. We also performed at the end of the self-consistency cycle a calculation in a MT potential, which gives a very small value for the $2p$ contribution to the efg of $V_{zz}^{2p} = -0.1 \times 10^{19}$ V/m². This shows that V_{zz}^{2p} is almost completely determined by the polarization of the $2p$ state under the influence of the non-spherical part of the effective potential and that the overlap of the p states of neighboring atoms plays only a minor role for the efg. For the reasons discussed in Sec. IV A, we did not perform a semicore calculation to determine the efg at the NN site of the Fe atom.

As in the case of Cu, we also performed a calculation with a 64-atom supercell in order to test the accuracy of the calculated efg's and asymmetry parameters. As an example we choose a substitutional V atom in Al since for this system the quadrupolar splittings of the nuclear levels of Al (nuclear spin $I = \frac{5}{2}$) are experimentally observed by means of the NQDOR technique³⁶ and because there is a large difference between the measured transition frequencies of the nuclei at the NN and next-NN sites of the V atom, which must be reproduced by the calculation. The relaxed atomic positions in units of a_0 are (0.488, 0.488, 0) for the first, (1.007, 0, 0) for the second, and (0.497, 0.497, 0.996) for the third shell. The two calculated quadrupolar transition frequencies per shell [corresponding to the transitions $|m| = \pm \frac{5}{2} \leftrightarrow \pm \frac{3}{2}$ (ν_2) and $\pm \frac{3}{2} \leftrightarrow \pm \frac{1}{2}$ (ν_1); see Ref. 37] and the asymmetry parameter of shells 1 and 2 are compared with the experimental values in Table V. We used $Q(^{27}\text{Al}) = 140 \times 10^{-31}$ m².^{38,39} Again there is good agreement between experiment and theory; in particular the large difference between the transition frequencies of the nuclei in shells 1 and 2 is well reproduced by the calculation.

C. efg in hexagonal Mg

As a last test case we choose the calculation of the efg at the nuclear sites in hexagonal magnesium (Mg). The calculations have been performed with the FLAPW method using 1020 \mathbf{k} points according to Monkhorst and Pack,⁴⁰ the tetrahedron method^{41,42} for the Brillouin-zone sampling, $G_c = 3.1$ a.u.⁻¹, $a_0 = 6.07$ a.u., and $c_0/a_0 = 1.62$. The calculation in

TABLE V. Quadrupolar transition frequencies of the Al nuclei near a substitutional V atom, calculated with the FLAPW method using 10 Chadi-Cohen \mathbf{k} points, $G_C=2.7$ a.u. $^{-1}$, and a relaxed 64-atom supercell. The core contribution ($1s$ - $2p$) to the efg has been calculated with the effective-potential method.

Shell	η	Theory			Experiment		
		ν_2 (kHz)	ν_1 (kHz)	$V_{zz}^{\text{core}}/V_{zz}^{\text{sph core}}$	η	ν_2 (kHz)	ν_1 (kHz)
1	0.05	1260	630	+0.08	0.12	1249	635
2	0	250	125	+0.12	0	220	110

which the $1s$ - $2p$ states of Mg are treated as spherically symmetric states gives $V_{zz}^{\text{sph core}}=3.67\times 10^{19}$ V/m 2 . The asymmetry parameter η vanishes by symmetry.

Using the effective-potential method to determine the core contribution to the efg at the end of the FLAPW cycle gives $V_{zz}^{\text{core}}=0.80\times 10^{19}$ V/m 2 , which is approximately 22% of $V_{zz}^{\text{sph core}}$. For the total efg we obtain $V_{zz}=4.47\times 10^{19}$ V/m 2 .

The Sternheimer function of Mg, considering the $1s$ - $2p$ states and calculated in the spherically symmetric part of the effective potential, is shown in Fig. 7. Outside the region of the core-charge density $\chi(r)$ takes the constant value $\gamma_{\infty}=-4.03$. Inserting the charge density of the FLAPW calculation with spherically symmetric $1s$ - $2p$ states in Eq. (46) gives $V_{zz}^{\text{core}}=0.84\times 10^{19}$ V/m 2 , in good agreement with the result of effective-potential method. The small difference between the two results may be caused by the fact that V_{zz}^{core} is calculated under the assumption that $\chi(r)$ is constant outside the MT sphere ($R_{\text{MT}}=2.95$ a.u.), although this is not exactly the case (see Fig. 7). A calculation in which the $2s$ and $2p$ states of Mg are treated with the help of local orbitals gives a contribution of these states to the efg of 0.67×10^{19} V/m 2 and a total efg of $V_{zz}=4.29\times 10^{19}$ V/m 2 .

Blaha, Schwarz, and Dederichs⁷ report on semicore calculations on hexagonal Mg. They showed that a calculation in which the $2s$ and $2p$ electrons are treated as semicore states gives a negligible contribution of these states to the efg. The reason for this large discrepancy to the results presented above is discussed in Sec. IV A. The value $V_{zz}^{\text{sph core}}=4.8\times 10^{19}$ V/m 2 reported in Ref. 7 is not comparable with our result since the authors used a smaller \mathbf{k} -point mesh (the efg depends sensitively on the number of \mathbf{k} points).

Our final result for the efg, $V_{zz}=4.5\times 10^{19}$ V/m 2 , is far from being converged with respect to the number of \mathbf{k} points; hence a comparison with the experimental value $V_{zz}^{\text{expt}}=\pm 5.3\times 10^{19}$ V/m 2 (Ref. 1) is not meaningful. However, the calculations show that considering the core contribution to the efg improves the agreement with experiment significantly.

V. SUMMARY AND CONCLUSIONS

In conventional band-structure calculations it is assumed that the charge density of the core states is spherically symmetric around the nuclear sites. Consequently, the core contribution to the efg is completely disregarded. The aim of the present paper was to show that the influence of closed elec-

tron shells on the electric-field gradient has to be considered in order to obtain reliable results for the total efg. We have presented two different methods for the computation of this core contribution to the efg, which yield identical results concerning the quadrupolar interaction energy with the nuclear quadrupole moment Q . These two methods can be applied at the end of the self-consistency cycle of a band-structure calculation with spherically symmetric core states, e.g., a FLAPW, FLMTO, PAW, pseudopotential calculation, and so on.

The first method treats the potential of the nuclear quadrupole moment as a perturbation for the spherically symmetric core-charge density. This perturbation induces an additional quadrupole moment in the core-charge density, which is given by $Q^{\text{ind}}(r)=-\gamma(r)Q$, with the Sternheimer function $\gamma(r)$. $\gamma(r)$ can be calculated using the spherically symmetric part of the effective potential by means of an inhomogeneous differential equation. The valence electrons and the neighboring nuclei at a distance r from the nucleus considered then interact locally with a local quadrupole moment $Q^{\text{tot}}(r)=[1-\gamma(r)]Q$. This leads to the fact that for the computation of the efg these charges have to be weighted with the factor $1-\gamma(r)$ in order to obtain the correct quadrupolar interaction energy with the nuclear quadrupole moment Q alone.

In the second method the Kohn-Sham equation of the core electrons is solved using the full nonspherical effective potential. This is done by expanding the core wave function into a suitably chosen basis set and solving the resulting eigenvalue problem numerically. As a consequence, the charge density of the core electrons is no longer spherically symmetric and the core contribution to the efg can be calculated directly.

The equivalence of these two methods concerning the quadrupolar interaction energy and hence the splitting of the nuclear levels (which is the quantity that is accessible experimentally) has been shown in Sec. III using second-order perturbation theory. It should be noted that the two methods give completely different results for the perturbation of the core wave function.

In Sec. IV we have calculated the efg at the nearest-neighbor sites of substitutional Ni (Fe) in Cu (Al) as well as the efg at the nuclear sites in hexagonal magnesium. In all these cases the core contribution to the efg is considerable and therefore should not be neglected. The theoretical transition frequencies in the neighborhood of a substitutional Pd (V) atom in Cu (Al), which we have computed using the results for the efg and the asymmetry parameter of a 64-atom supercell calculation and tabulated values for the nuclear quadrupole moment, are in good agreement with the frequencies obtained by means of NQDOR measurements.

Up to now it has been assumed that, in combination with the FLAPW method, the contribution of the highest core states (e.g., of $3s$ and $3p$ states of Cu) to the efg can be computed reliably with the help of semicore calculations. However, in Sec. IV A we showed that semicore calculations are not suited for the determination of the core contribution to the efg due to the limited basis set inside the MT spheres. The resulting core contributions are often an order of magnitude too small. Contrarily, the results of FLAPW calcula-

tions with local orbitals are in good agreement with the results of the two methods presented in this paper. The reason for this is that in calculations with local orbitals the core electrons are treated together with the valence electrons in the same energy window and that the perturbation of the core wave functions by the nonspherical part of the effective potential can be described by the augmentation functions of the

FLAPW basis set for the valence wave functions inside the MT spheres.

ACKNOWLEDGMENTS

The authors are indebted to A. Seeger, H. Krimmel, and P. Blaha for helpful discussions. Part of the calculations were performed at the HLRZ in Jülich.

-
- ¹E. N. Kaufmann and R. J. Vianden, *Rev. Mod. Phys.* **51**, 161 (1979).
- ²H. Haas, *Z. Naturforsch. Teil A* **41**, 78 (1986).
- ³A. Seeger, J. Ehmann, and M. Fähnle, *Z. Naturforsch. Teil A* **51**, 489 (1996).
- ⁴R. M. Sternheimer, *Z. Naturforsch. Teil A* **41**, 24 (1986).
- ⁵P. Hohenberg and W. Kohn, *Phys. Rev.* **136**, B864 (1964).
- ⁶W. Kohn and L. J. Sham, *Phys. Rev.* **140**, A1133 (1965).
- ⁷P. Blaha, K. Schwarz, and P. H. Dederichs, *Phys. Rev. B* **37**, 2792 (1988).
- ⁸M. Methfessel and S. Frota-Pessôa, *J. Phys. Condens. Matter* **2**, 149 (1990).
- ⁹B. Drittler, M. Weinert, R. Zeller, and P. H. Dederichs, *Phys. Rev. B* **42**, 9336 (1990).
- ¹⁰K. Schwarz, C. Ambrosch-Draxl, and P. Blaha, *Phys. Rev. B* **42**, 2051 (1990).
- ¹¹S. Ferreira and S. Frota-Pessôa, *Phys. Rev. B* **51**, 2045 (1995).
- ¹²P. Blaha, D. Singh, P. I. Sorantin, and K. Schwarz, *Phys. Rev. B* **46**, 1321 (1992).
- ¹³S. Buck, K. Hummler, and M. Fähnle, *Phys. Status Solidi B* **195**, K9 (1996).
- ¹⁴D. Singh and H. Krakauer, *Phys. Rev. B* **43**, 1441 (1991).
- ¹⁵K. Hummler and M. Fähnle, *Phys. Status Solidi B* **186**, K11 (1994).
- ¹⁶K. Hummler and M. Fähnle, *Phys. Rev. B* **53**, 3272 (1996).
- ¹⁷K. Hummler and M. Fähnle, *Phys. Rev. B* **53**, 3290 (1996).
- ¹⁸P. Blaha, K. Schwarz, P. Dufek, and R. Augustyn, WIEN95, Technical University of Vienna, 1995, improved and updated Unix version of the original copyrighted WIEN code of Ref. 26.
- ¹⁹D. Singh, *Planewaves, Pseudopotentials and the LAPW Method* (Kluwer, Dordrecht, 1994).
- ²⁰D. Singh, *Phys. Rev. B* **43**, 6388 (1991).
- ²¹D. D. Koelling and G. O. Arbman, *J. Phys. F* **5**, 2041 (1975).
- ²²O. K. Andersen, *Phys. Rev. B* **12**, 3060 (1975).
- ²³W. E. Pickett, *Comput. Phys. Rep.* **9**, 115 (1989).
- ²⁴P. E. Blöchl, *Phys. Rev. B* **50**, 17 953 (1994).
- ²⁵B. Meyer, K. Hummler, C. Elsässer, and M. Fähnle, *J. Phys. Condens. Matter* **7**, 9201 (1995).
- ²⁶P. Blaha, K. Schwarz, P. Sorantin, and S. B. Trickey, *Comput. Phys. Commun.* **59**, 399 (1990).
- ²⁷G. D. Gaspari, W.-M. Shyu, and T. P. Das, *Phys. Rev.* **134**, A852 (1964).
- ²⁸M. H. Cohen and F. Reif, in *Solid State Physics* (Academic, New York, 1957), Vol. 5, p. 321.
- ²⁹F. D. Feiok and W. R. Johnson, *Phys. Rev.* **187**, 39 (1969).
- ³⁰M. Minier and C. Minier, *Phys. Rev. B* **22**, 21 (1980).
- ³¹D. J. Chadi and M. L. Cohen, *Phys. Rev. B* **8**, 5747 (1973).
- ³²C. L. Fu and K. M. Ho, *Phys. Rev. B* **28**, 5480 (1983).
- ³³K. Konzelmann, G. Majer, and A. Seeger, *Z. Naturforsch. Teil A* **51**, 506 (1996).
- ³⁴R. Nevald and G. Petersen, *J. Phys. F* **5**, 1778 (1975).
- ³⁵B. Effenberger, W. Kunold, W. Oesterle, M. Schneider, L. M. Simons, R. Abela, and J. Wüest, *Z. Phys. A* **309**, 77 (1982).
- ³⁶C. Berthier and M. Minier, *J. Phys. F* **7**, 515 (1977).
- ³⁷T. P. Das and E. L. Hahn, in *Solid State Physics* (Academic, New York, 1958), Suppl. 1, p. 1.
- ³⁸P. Pyykkö, *Z. Naturforsch. Teil A* **47**, 189 (1992).
- ³⁹D. Sundholm and J. Olsen, *Phys. Rev. Lett.* **68**, 927 (1992).
- ⁴⁰H. J. Monkhorst and J. D. Pack, *Phys. Rev. B* **13**, 5188 (1976).
- ⁴¹O. Jepsen and O. K. Andersen, *Solid State Commun.* **9**, 1763 (1971).
- ⁴²G. Lehmann and M. Taut, *Phys. Status Solidi B* **54**, 469 (1972).